pISSN 1229-845X, eISSN 1976-555X
*J. Vet. Sci.* (2012), **13**(3), 299-310
http://dx.doi.org/10.4142/jvs.2012.13.3.299
Received: 5 Aug. 2011, Accepted: 17 Mar. 2012

JOURNAL OF
Veterinary
Science

**Original Article**

# Comparing the osteogenic potential of canine mesenchymal stem cells derived from adipose tissues, bone marrow, umbilical cord blood, and Wharton's jelly for treating bone defects

**Byung-Jae Kang[1,†], Hak-Hyun Ryu[1,†], Sung Su Park[1], Yoshihisa Koyama[2], Masanori Kikuchi[2], Heung-Myong Woo[3], Wan Hee Kim[1], Oh-Kyeong Kweon[1,*]**

[1]*Department of Veterinary Surgery, College of Veterinary Medicine, Seoul National University, Seoul 151-742, Korea*
[2]*Biomaterials Center, National Institute for Materials Science, Ibaraki 305-0044, Japan*
[3]*College of Veterinary Medicine and KNU Stem Cell Institute, Kangwon National University, Chuncheon 200-701, Korea*

**Alternative sources of mesenchymal stem cells (MSCs) for replacing bone marrow (BM) have been extensively investigated in the field of bone tissue engineering. The purpose of this study was to compare the osteogenic potential of canine MSCs derived from adipose tissue (AT), BM, umbilical cord blood (UCB), and Wharton's jelly (WJ) using *in vitro* culture techniques and *in vivo* orthotopic implantation assays. After canine MSCs were isolated from various tissues, the proliferation and osteogenic potential along with vascular endothelial growth factor (VEGF) production were measured and compared *in vitro*. For the *in vivo* assay, MSCs derived from each type of tissue were mixed with β-tricalcium phosphate and implanted into segmental bone defects in dogs. Among the different types of MSCs, AT-MSCs had a higher proliferation potential and BM-MSCs produced the most VEGF. AT-MSCs and UCB-MSCs showed greater *in vitro* osteogenic potential compared to the other cells. Radiographic and histological analyses showed that all tested MSCs had similar osteogenic capacities, and the level of new bone formation was much higher with implants containing MSCs than cell-free implants. These results indicate that AT-MSCs, UCB-MSCs, and WJ-MSCs can potentially be used in place of BM-MSCs for clinical bone engineering procedures.**

**Keywords:** cell source, dogs, mesenchymal stem cells, osteogenesis

## Introduction

Large segmental bone defects caused by events such as trauma, inflammation, or cancer result in serious functional problems, and repair of these injuries is a significant challenge in reconstructive surgery [8,35]. The current gold standard for repairing bone defects is bone graft transplantation despite considerable efforts to develop new therapeutic approaches [22]. This widely-used strategy generally results in a positive clinical outcome, but has many disadvantages including significant morbidity at the donor site, limited supply of bone tissue, increased blood loss, more surgical procedures, decreased osteogenic potential of the grafted bone, potential risk of infection, and problematic immune responses after implantation [8,14]. For these reasons, bone tissue engineering procedures using a combination of mesenchymal stem cells (MSCs) derived from various sources and biomaterials have been investigated as a replacement for more conventional bone graft techniques [7,20].

MSCs are multipotent cells capable of differentiating into various cell types such as osteoblasts, chondrocytes, adipocytes, myoblasts, tenoblasts, and neuronal cells [9,14,30,33]. MSCs have received extensive attention in the fields of tissue engineering and regenerative medicine because they can be easily harvested in a minimally invasive manner, propagate *in vitro*, and possess valuable properties such as multipotency, paracrine activities, and immune modulation abilities [3,18,30]. In particular, the osteogenic potential of MSCs for repairing bone defects

*Corresponding author: Tel: +82-2-880-1248; Fax: +82-2-888-2866; E-mail: ohkweon@snu.ac.kr
†The first two authors contributed equally to this work.

ⓒ 2012 The Korean Society of Veterinary Science.
This is an Open Access article distributed under the terms of the Creative Commons Attribution Non-Commercial License (http://creativecommons.org/licenses/by-nc/3.0) which permits unrestricted non-commercial use, distribution, and reproduction in any medium, provided the original work is properly cited.

has been evaluated by many researchers [6,25,28,29]. However, careful selection of the most suitable cell source and development of other treatment protocols are needed to achieve more satisfactory bone regeneration results [14].

Currently, it is unclear which type of MSCs is the most suitable for promoting bone regeneration or whether MSCs derived from various tissues have a similar potential for inducing bone formation. Bone marrow (BM) is the most common and readily available cell source for bone engineering procedures, but harvesting this tissue is painful and laborious [8,12,14]. In addition to BM, other tissues including adipose tissue (AT), muscle, umbilical cord blood (UCB), placenta, and Wharton's jelly (WJ) may be sources of MSCs appropriate for bone engineering techniques [3,13,15,27,31].

The purpose of this study was to compare the osteogenic potential of canine MSCs derived from AT, BM, UCB, and WJ. We assessed the cumulative population doubling level (CPDL), mineralization capability, alkaline phosphatase (ALP) activity, and vascular endothelial growth factor (VEGF) production of these MSCs using an *in vitro* culture assay. The osteogenic ability of the cells was also evaluated using an *in vivo* orthotopic implantation assay.

## Materials and Methods

### Animals

Twenty healthy beagle dogs (13 males and 7 females), aged approximately 2 years old with the mean weight of 10.1 ± 1.8 kg were used for the present experiment. The dogs were housed in an indoor facility located in Veterinary Medical Teaching Hospital of Seoul National University, Korea. All animal experimental procedures were approved by the Institutional Animal Care and Use Committee of Seoul National University (SNU-090623-1), Korea.

### Isolation and cultivation of canine MSCs

Canine MSCs were obtained from gluteal subcutaneous fat, BM aspirates, WJ, and UCB.

AT was aseptically collected from subcutaneous fat. The fat tissues weighing around 1 g were washed extensively with phosphate-buffered saline (PBS) (Gibco, USA), minced, and digested with collagenase type I (1 mg/mL) at 37°C for 1 h with intermittent shaking. The suspension was filtered through a 100-μm nylon mesh and centrifuged at 200 × g for 10 min to separate floating adipocytes from stromal cells. Pre-adipocytes in the stromal vascular fraction were plated in T75 flasks (Thermo Fisher Scientific, USA) at a density of $1 \times 10^5$ cells/cm$^2$.

BM was aseptically collected from the humeral bone with BM biopsy needle (CareFusion, USA) and 10 mL syringe under anesthesia. The BM was placed in tubes (BD Biosciences, USA) that were treated with an anti-coagulant. The marrow was diluted 1 : 1 with PBS. A Ficoll-Paque plus (Amersham Biosciences, Sweden) density gradient was then used to collect the buffy coat layer. The diluted marrow was gently placed on Ficoll-Paque solution and centrifuged at 400 × g for 20 min. Cells from the buffy coat were washed with PBS and centrifuged at 200 × g for 10 min. The pellets were resuspended in PBS, and the cells were plated in T75 flasks at a density of $1 \times 10^5$ cells/cm$^2$.

Fresh canine umbilical cords were obtained after cesarean sections and placed in 20 mL of Hanks' balanced salt solution (HBSS) (Gibco, USA) at 4°C. Following disinfection in 70% ethanol for 30 sec, the umbilical cord vessels were removed while still in HBSS. The mesenchymal tissue (in WJ) was then minced into pieces about 20 mm$^3$ in size and centrifuged at 200 × g for 5 min. After removing the supernatant fraction, the pellet (mesenchymal tissue) was washed with serum-free Dulbecco's modified Eagle's medium (DMEM) (Gibco, USA), and centrifuged at 200 × g for 5 min. The supernatant was aspirated and the mesenchymal tissue was incubated with collagenase type I (1 mg/mL) at 37°C for 12 h, washed with PBS, and further digested with 2.5% trypsin (Gibco, USA) at 37°C for 30 min. Fetal bovine serum (FBS) (Hyclone, USA) was then added to the mesenchymal tissue to stop trypsinization. The cells were plated in T75 flasks at a density of $1 \times 10^5$ cells/cm$^2$.

Low-density mononuclear cells were isolated from UCB using a Ficoll-Paque density gradient. The diluted UCB was gently placed on Ficoll-Paque solution and centrifuged at 400 × g for 20 min. The cells were washed with PBS and centrifuged at 200 × g for 10 min. The pellets were resuspended in PBS and the cells plated in T75 flasks at a density of $1 \times 10^5$ cells/cm$^2$.

All the cells isolated from each type of tissue were incubated overnight in DMEM supplemented with 10% FBS at 37°C in a humidified atmosphere of 5% $CO_2$. Unattached cells were removed after 24 h by washing with PBS, and cell medium was replaced with fresh medium every 2 days until the cells were confluent. When the confluence was more than 90%, the cells were cryopreserved at −150°C or subcultured.

### Flow cytometry analysis

Trypsinized MSCs were suspended in PBS containing 5% bovine serum albumin (Sigma-Aldrich, USA) at a concentration of $5 \times 10^5$ cells/30 μL. The cells were stained with fluorescein isothiocyanate (FITC)-conjugated antibodies specific for CD14 (clone CAM36A; VMRD, USA), CD34 (clone 1H6; Serotec, UK), CD45 (clone CADO18A; VMRD, USA), and CD105 (clone SN6; Serotec, UK) at 4°C for 30 min. The cells were also incubated with phycoerythrin (PE)-conjugated antibodies against CD44 (clone IM7; Abcam, UK), CD73 (clone 7G2; Abcam, UK), and CD90 (clone DH2A; VMRD, USA) at 4°C for 30 min. Negative control cells were stained with a FITC-conjugated

mouse IgG1 isotype (Invitrogen, USA) or a PE-conjugated mouse IgG1 isotype antibodies (Invitrogen, USA) at 4°C for 30 min. Expression of the corresponding cell surface markers was evaluated with a FACS Calibur flow cytometer (BD Biosciences, USA) using CELL Quest Pro (BD Biosciences, USA) software.

**Comparison of proliferation potential**

CPDL was calculated using the formula "$\chi = \{\log_{10}(N_H) - \log_{10}(N_1)\}/\log_{10}(2)$" [24] in which $N_1$ is the inoculum cell number and $N_H$ is the cell harvest number. To determine the cumulated doubling level, the population doubling level for each passage was calculated and then added to the levels of the previous passages. Since the number of isolated cells from all tissues could be determined for the first time at passage 1, the cumulative doubling number was first calculated for passage 1.

**Osteogenic differentiation**

Various MSCs from the third passage were cultured in low-glucose DMEM (Sigma-Aldrich, USA) supplemented with 10% FBS in 6-well plates (Thermo Fisher Scientific, USA) at a cell density of $1 \times 10^4/cm^2$. The DMEM was then replaced with osteogenic medium composed of low-glucose DMEM supplemented with 10% FBS, 0.1 μM dexamethasone (Sigma-Aldrich, USA), 50 μM ascorbic acid-2-phophate (Sigma-Aldrich, USA), and 10 mM beta-glycerophosphate (Sigma-Aldrich, USA), and the cells were incubated for 14 days.

**Quantification of mineralization**

Alizarin Red S staining was used to observe calcium mineralization. For this procedure, all the different types of MSCs incubated in 6-well plates with osteogenic medium for 14 days were washed twice with distilled water (DW) and fixed in a solution of ice-cold 70% ethanol for 1 h. After being carefully washing five times with DW and then for 15 min with PBS, the cells were stained for 10 min with 40 mM Alizarin Red S (Sigma-Aldrich, USA) at room temperature. Unincorporated dye was removed by aspiration, and the wells were washed four times with 4 mL DW for 5 min with shaking. The plates were then left at an angle for 2 min to remove excess water, re-aspirated, and stored at −20°C prior to dye extraction. Stained monolayers were visualized by phase contrast microscopy using an inverted microscope (Nikon, Japan). For staining quantification, cells stained with Alizarin Red S were solubilized in cetylpyridinium chloride (1 mL; Sigma-Aldrich, USA) for 1 h as previously described [16]. Absorbance of solubilized Alizarin Red S was measured at 570 nm using a spectrophotometer (SmartSpec 3000 Spectrometer; Bio-Rad, USA).

**Measurement of ALP activity**

The ALP activity was measured using an ALP assay kit (Takara Bio, Japan) according to the manufacturer's instructions. In brief, a *p*-nitro-phenyl phosphate (PNPP) solution was prepared by dissolving 24 mg of PNPP substrate in 5 mL ALP buffer. The cells were lysed by adding 500 μL of extraction solution to each well. The cleared supernatant was collected after centrifugation at 16,000 × g at 4°C for 10 min. The cell lysate supernatant was mixed with 50 μL of PNPP substrate solution and incubated at 37°C for 30 min. Stop solution (50 μL, 0.9 N NaOH) was added to each well and the absorbance was measured at 405 nm with a spectrophotometer after color development.

**Measurement of VEGF**

MSCs were seeded in 75 $cm^2$ flasks with DMEM containing 2% FBS and incubated at 37°C in a humidified atmosphere of 5% $CO_2$. Cultured media was collected after 48 h of incubation. Levels of VEGF in the media were then measured using an enzyme-linked immunosorbent assay kit (Quantikine Canine VEGF; R&D Systems, USA) according to the manufacturer's instructions. The same medium was used as the negative control. The absorbance was measured at 450 nm using a spectrophotometer.

**Preparation of the bioceramic scaffold**

A β-TCP/poly L-lactide-*co*-glycolide-*co*-ε-caprolactone (TCP/PLGC) composite membrane and β-TCP granules were synthesized and provided from the Biomaterial Center, National Institute for Material Science, Japan [7,24]. Briefly, an $H_3PO_4$ aqueous solution (5 $dm^3$, 0.67 M) was gradually added to a 1 M $Ca(OH)_2$ suspension with vigorous stirring. pH of the reaction was maintained at 6～7 by the addition of a 28% ammonium aqueous solution. The precipitate was dried at 120°C and burned at 800ºC. The resulting TCP block was crushed into granules. Granules with a particle size between 500 and 1,000 μm were collected by sieve classification. Granules were identified by powder X-ray diffraction (PW-1700 system; Royal Philips Electronics, Netherlands).

PLGC was synthesized by bulk copolymerization of L-lactide, glycolide, and ε-caprolactone using stannous 2-ethylhexanoate. TCP/PLGC composite was synthesized by mixing TCP and PLGC in a weight ratio of 7 : 3 at 180°C for 10 min. The composite was formed into membranes with a thickness of 200 μm using a hot press (Mini Test Press; Toyo Seiki, Japan) at 180°C.

**Orthotopic implantation**

The mean diameter of the mid-portion of the radial diaphysis was determined by radiography to create a segmental defect with the critical size in the radial diaphysis. Because the mean diameter of the mid-portion of the radial diaphysis was less than 10 mm, the animals underwent a unilateral resection that created a segmental

defect 15-mm long in the radial diaphysis as previously described [2,6]. In brief, the dogs were sedated with intravenous administration of acepromazine maleate (Sedaject; Samwoo Medical, Korea) at a dose of 0.05 mg/kg of body weight. Anesthesia was then induced with the intravenous delivery of 1% propofol (Provive 1%; Claris Lifesciences, India) at a dose of 6 mg/kg of body weight and maintained with isoflurane (Aerrane; Baxter, Canada) in oxygen. Tramadol (Toranzin; Samsung Pharmaceutical, Korea) administered intravenously at a dose of 4 mg/kg of body weight was used as an analgesic. Anesthesia monitor (Datex-Ohmeda; Microvitec Display, UK) was used to monitor physiologic factors including rectal temperature, oxygen saturation, end tidal $CO_2$, electrocardiogram, minimum alveolar concentration value, and pulse rate. Under sterile conditions, a craniomedial incision was made in the skin to expose the diaphysis of the right radius (Fig. 1). An eight-hole, 2.7 dynamic compression plate (Synthes, Switzerland) was contoured and placed on the cranial aspect of the radius. The plate then was removed, and a 15 mm-long segmental defect was made at the mid-portion of the diaphysis using an oscillating saw (Stryker, USA).

The defect was filled with a mixture of β-TCP plus AT-MSCs (AT-MSC group, n = 4), β-TCP plus BM-MSCs (BM-MSC group, n = 4), β-TCP plus UCB-MSCs (UCB-MSC group, n = 4), β-TCP plus WJ-MSCs (WJ-MSC group, n = 4), or β-TCP alone (control group, n = 4). MSCs ($1 \times 10^6$, third passage) transplanted into each experimental group were suspended in 700 μL of normal saline and mixed with 700 mg β-TCP just before implantation. An appropriate volume of saline was mixed with β-TCP for the control group. The site of implantation was covered with a TCP/PLGC composite membrane. After the plate was reapplied, the fascia and skin were closed. All surgical procedures were performed under the same conditions. Two weeks after surgery, all dogs were able to walk and bear weight using the right antebrachium.

## Radiographic examination

Anteroposterior and mediolateral radiographs of the right antebrachium were taken before and immediately after the operation as well as 4, 8, 12, 16, and 20 weeks postoperatively. All of the radiographs were evaluated to identify the presence of osseous union at each host bone-implant interface and monitor changes in implant radiopacity. Bone union at the host bone-implant interfaces was identified by obliteration of the transverse radiolucent line between the host bone and implant that was observed immediately after surgery. The time at which bone healing was observed at the host bone-implant interfaces was also recorded.

## Histological and histomorphometric analysis

For histological analysis, the implants of all groups were harvested 20 weeks after the operation. Segments of each radius including the implanted site were excised and fixed in 4% paraformaldehyde. The specimens then were decalcified with 15% formic acid in PBS for 6 to 12 weeks. After decalcification, the segments were dehydrated in a series of ethanol solutions and embedded in paraffin. Longitudinal sections 5-μm thick were cut (Reichert-Jung, Germany) in the coronal plane. These sections were stained with hematoxylin and eosin or azocarmine and aniline blue to observe new bone formation. Stained sections from each group were examined by light microscopy (Olympus, Japan) and photographed using an attached digital camera (Nikon, Japan). For histomorphometric analysis, sizes of the newly formed bone area (NBA) and residual β-TCP area (RTA) were estimated and converted into a percentage of the total implanted area (TA) using an image processing and analysis program (ImageJ; National Institutes of Health, USA).

## Statistical analysis

Data were analyzed using SPSS statistical analytical software (ver. 18.0; IBM, USA). A Kruskal-Wallis test was used to assess differences among the groups. A post-hoc test was performed along with a Mann-Whitney U test. *p*-values less than 0.05 were considered to be statistically significant.

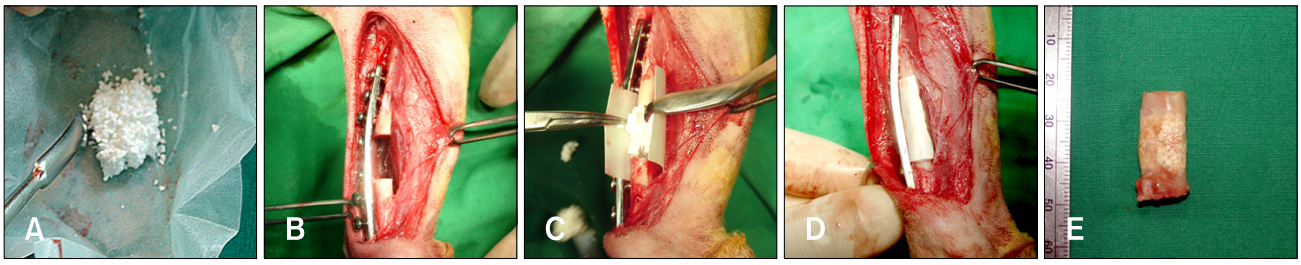


**Fig. 1.** The orthotopic implantation procedure. (A) β-tricalcium phosphate (β-TCP) mixed with canine mesenchymal stem cells (MSCs). (B) Segmental defect in the radial diaphysis. (C) Filling the bone defect with β-TCP compound and MSCs. (D) Complete implantation. (E) Implant harvested after 20 weeks.

## Results

### Establishment of canine MSCs from various tissues

Canine MSCs derived from AT, BM, UCB, and WJ were cultured under basal conditions and their cell morphologies at the third passage were compared. Generally, all cells formed a monolayer consisting of spindle-shaped cells (Figs. 2A ~ D). Fluorescence-activated cell sorting analysis was used to identify cell surface markers on the canine MSCs at the third passage. All cells had the same phenotype and were positive for CD44, CD73, CD90, and CD105 but negative for hematopoietic and endothelial markers including CD14, CD34, and CD45 (Figs. 2E and F).

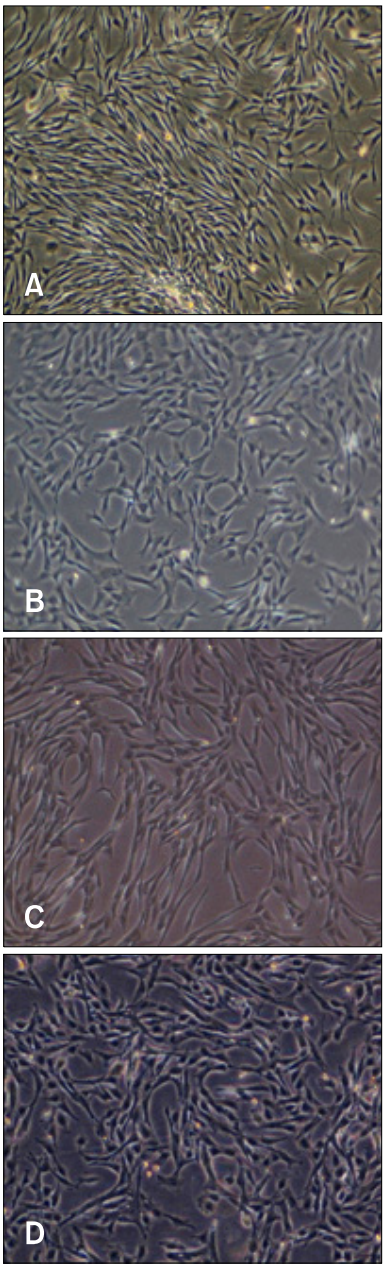


E

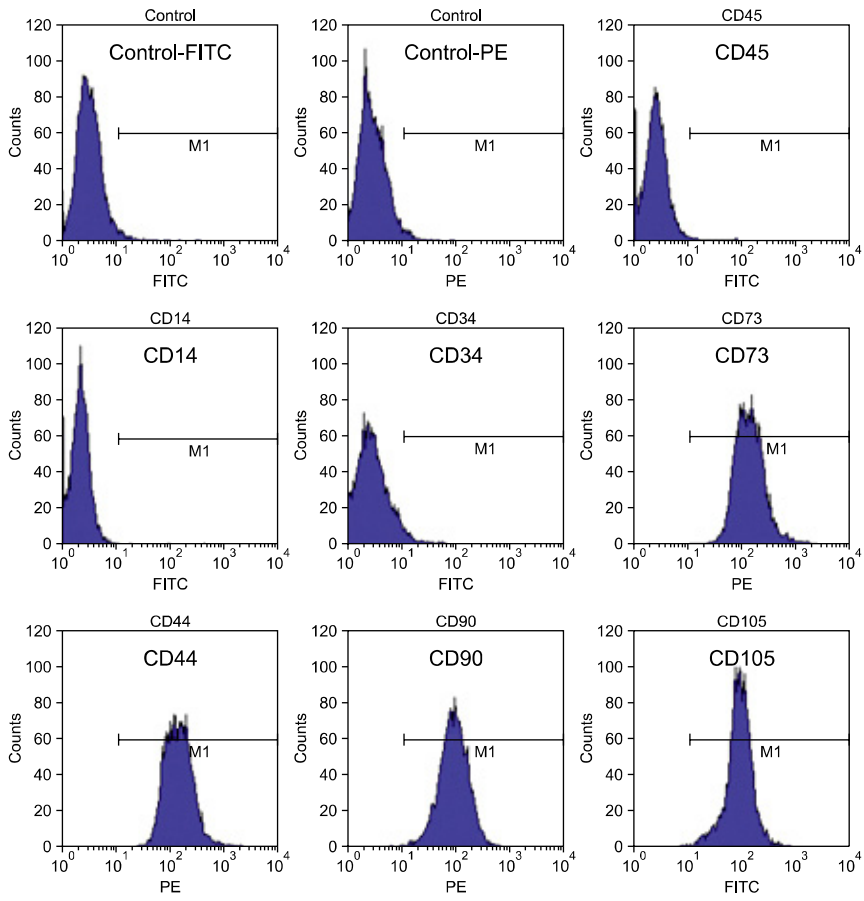


F

| Group | AT-MSCs | BM-MSCs | UCB-MSCs | WJ-MSCs |
|---|---|---|---|---|
| CD14 | − | − | − | − |
| CD34 | − | − | − | − |
| CD44 | + | + | + | + |
| CD45 | − | − | − | − |
| CD73 | + | + | + | + |
| CD90 | + | + | + | + |
| CD105 | + | + | + | + |

**Fig. 2.** Morphologic comparison and fluorescence-activated cell sorting (FACS) analysis of various cultured canine MSCs at passage 3. MSCs were isolated from different tissues including (A) adipose tissue (AT), (B) bone marrow (BM), (C) umbilical cord blood (UCB) and (D) Wharton's jelly (WJ). All the cells had a typical fibroblast-like morphology. (E and F) FACS analysis revealed that AT-MSCs, BM-MSCs, UCB-MSCs, and WJ-MSCs expressed CD44, CD73, CD90, and CD105 but not CD14, CD34, or CD45. A ~ D: ×40. FITC: fluorescein isothiocyanate, PE: phycoerythrin.

### Proliferation potential of canine MSCs from various tissues

Analysis of the canine MSCs proliferation potential revealed that WJ-MSCs had the lowest population doubling numbers through passages 2 ~ 5, but BM-MSCs showed the lowest doubling numbers after passage 7 (Fig. 3). AT-MSCs possessed the highest population doubling numbers at all passages. After passage 6, AT-MSCs had the highest proliferation capacity followed by UCB-MSCs and WJ-MSCs while BM-MSCs had the lowest proliferation potential (Fig. 3).

### Comparison of *in vitro* osteogenic potential

To evaluate the *in vitro* osteogenic differentiation potential of the MSCs, confluent cultures of AT-MSCs, BM-MSCs, UCB-MSCs, and WJ-MSCs were maintained in osteogenic

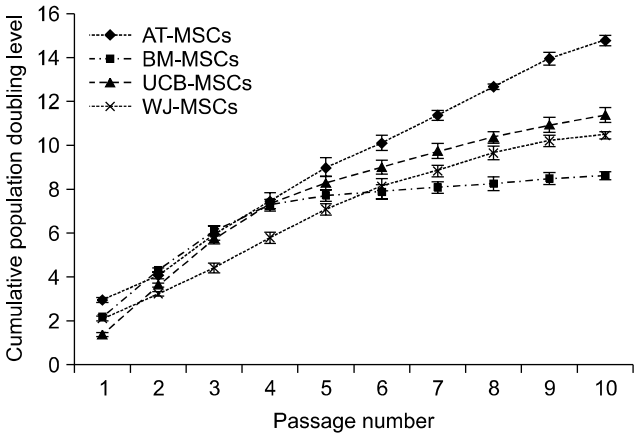


**Fig. 3.** Cumulative population doubling levels of canine MSCs derived from various tissues. Population doubling was measured at each passage. Data are expressed as the mean ± SD (n = 3).

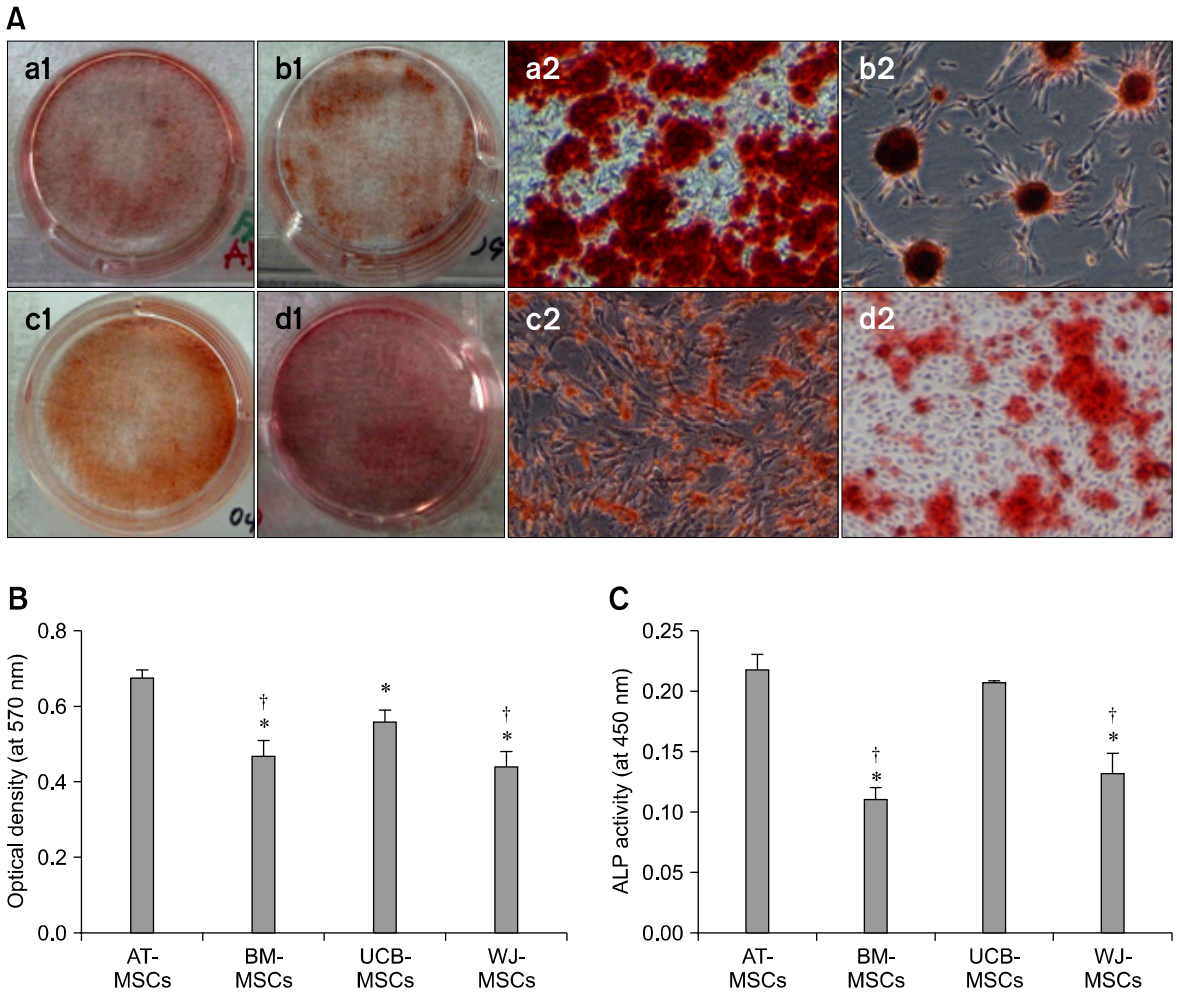


**Fig. 4.** Mineralization assay results and alkaline phosphatase (ALP) activity of the various MSCs. (A) AT-MSCs (a1 and a2), BM-MSCs (b1 and b2), UCB-MSCs (c1 and c2), and WJ-MSCs (d1 and d2) were seeded and cultured in osteogenic medium for 2 weeks after the cells reached confluence. To confirm the presence of calcium deposits, cells were stained with Alizarin Red S. Quantification of mineralization (B) and ALP activity (C) was performed to compare *in vitro* osteogenic capabilities of the MSCs. Data are presented as the mean ± SD (n = 3). *Indicates a statistically significant difference ($p < 0.05$) compared to the AT-MSCs under the same conditions. †Indicates a statistically significant difference ($p < 0.05$) compared to the UCB-MSCs. a2, b2, c2, and d2: ×40.

induction medium for 2 weeks. All the cells generated a large number of mineral nodules within this time. The cells were fixed and stained with Alizarin Red S to visualize the deposition of calcium-rich granules on the cell surface. Intense staining was seen in all MSCs (Fig. 4A). The degree of Alizarin Red S staining was greater in AT-MSCs and UCB-MSCs than BM-MSCs and WJ-MSCs after 2 weeks of subculturing under osteogenic differentiation conditions (Fig. 4B). ALP activity, which is recognized as an early osteoblastic marker, was also measured. Levels of ALP activities of AT-MSCs and UCB-MSCs were significantly greater than those of BM-MSCs and WJ-MSCs ($p < 0.05$, Fig. 4C).

## Quantitative analysis of VEGF production

The amount of secreted VEGF, a signal protein produced by cells that stimulate vasculogenesis and angiogenesis, was measured. After 48 h of incubation, VEGF production of the BM-MSCs was significantly greater than that of the other types of MSCs ($p < 0.05$, Fig. 5). VEGF production of the AT-MSCs was less than that of UCB-MSCs and WJ-MSCs ($p < 0.05$, Fig. 5).

## Radiographic analysis

Representative radiographs for each group of dogs taken at 0, 4, 12, and 20 weeks after surgery are shown in Fig. 6. The β-TCP powder implanted in the bone defects was easily visualized on X-ray images. Over time, implants that had a granular appearance immediately after the operation developed a smoother and more radiopaque appearance in all groups. This was because mineralized tissue had formed in the empty space among the scaffolds as new bone was formed.

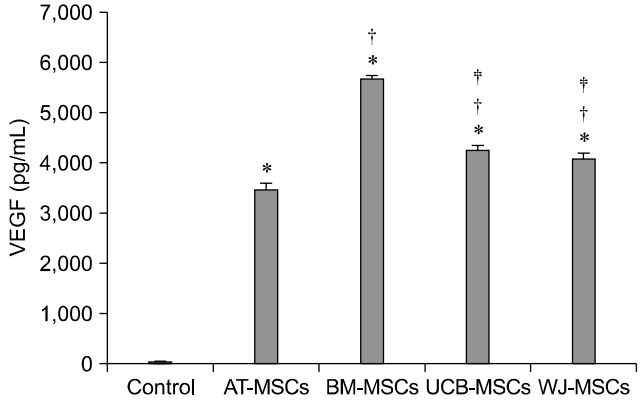


**Fig. 5.** Quantification of vascular endothelial growth factor (VEGF) produced by the various MSCs. Data are presented as the mean ± SD (n = 3). *Indicates a statistically significant difference ($p < 0.05$) compared to the control under the same conditions. †Indicates a statistically significant difference ($p < 0.05$) compared to the AT-MSCs. ‡Indicates a statistically significant difference ($p < 0.05$) compared to the BM-MSCs.

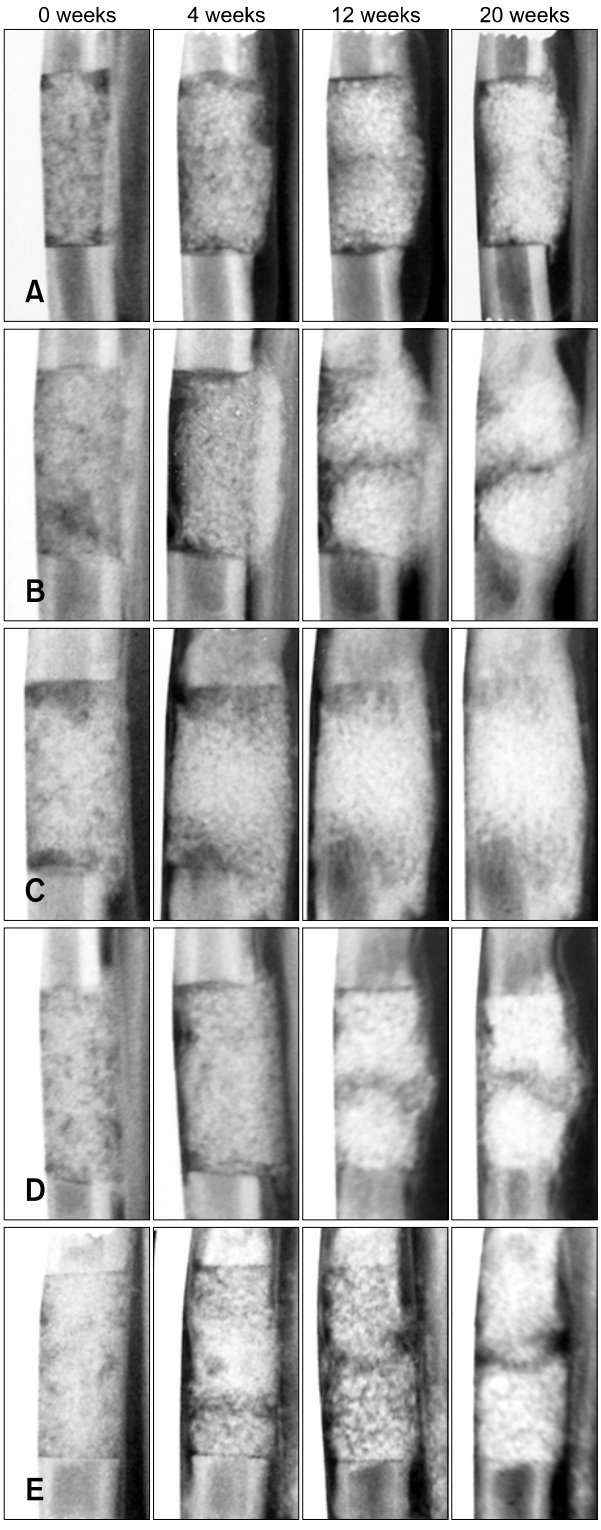


**Fig. 6.** Mediolateral radiographs of the treated defects obtained immediately after the operation as well as 4, 12, and 20 weeks after surgery. The radiolucent transverse zone at the defect ends remained distinct in the control group (A) after 20 weeks. In contrast, union at the host bone-implant interfaces was evident in the AT-MSC (B), BM-MSC (C), UCB-MSC (D), and WJ-MSC (E) groups.

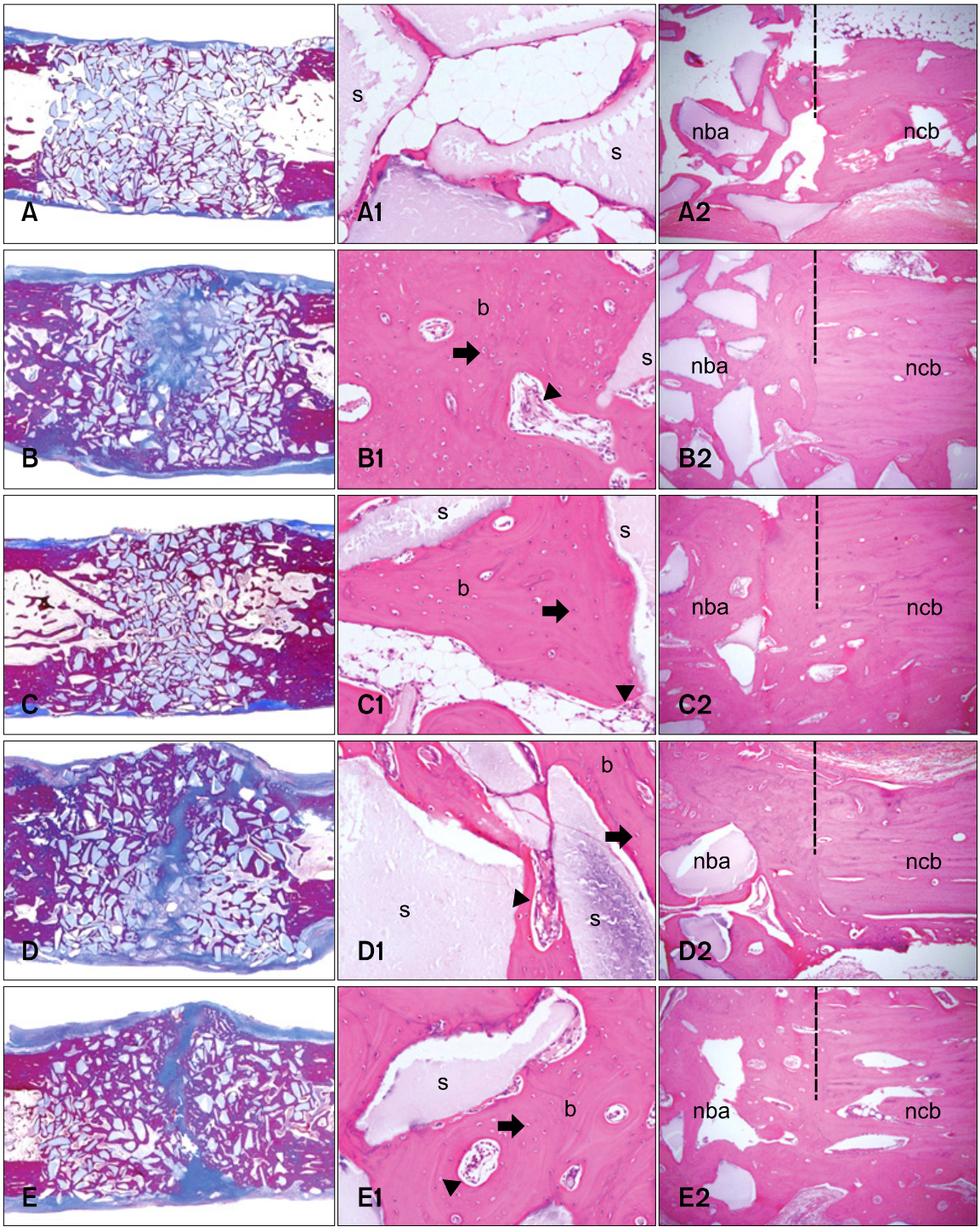


**Fig. 7.** Coronal sections of the segmental bone defects 20 weeks after implantation. Macroscopic views of the repaired area in each group are shown: (A) control, (B) AT-MSC, (C) BM-MSC, (D) UCB-MSC, and (E) WJ-MSC groups. The proximal portion is at the left of the panels (A ~ E). Bone was stained purple and residual β-TCP was light blue. Bone formation was observed on the surface the β-TCP throughout the defect in all groups. However, there was a higher amount of bone formation in all experimental groups compared to the control animals. Detailed views of the inside (A1, B1, C1, D1, and E1) and interfacial (A2, B2, C2, D2, and E2) areas are shown. In the control group, a minimal amount of new bone was observed in the inside area (A1), and cortical continuity was not found at the interfacial area (A2). In the experimental groups, osteocytes (arrow) and hematopoietic tissues (arrow head) embedded in substantial bone matrix were found together with some intact β-TCP particles in the inside area (B1, C1, D1, and E1). Cortical bony bridging had also formed at the interfacial area (B2, C2, D2, and E2). AZAN (A ~ E) and H&E (A1, 2, B1, 2, C1, 2, D1, 2, E1, and 2) stain. A1, B1, C1, D1, and E1: ×200, A2, B2, C2, D2, and E2: ×40. b: bone, s: β-TCP scaffold, ncb: native cortical bone area, nba: newly formed bone area.

**Table 1.** Radiographic analysis at the host bone-implant interfaces for each group

| | Control | AT-MSC | BM-MSC | UCB-MSC | WJ-MSC |
|---|---|---|---|---|---|
| Radiographic healing (healed/total interfaces) | 1/8 | 6/8 | 7/8 | 7/8 | 7/8 |
| Bone union period* (week) | − | 14.67 ± 3.27 | 13.71 ± 3.15 | 11.43 ± 2.76 | 13.71 ± 2.14 |

*Bone union periods indicative of healing at the host bone-implant interface are expressed as the mean ± SD. The control group was excluded from calculating this period because only one interface had healed as observed on the radiographs. No significant differences in the bone union period were found among the experimental groups.

A transverse radiolucent line between the host bone and implant was also seen in radiographs taken immediately after the operation. Obliteration of this line was regarded as radiographic evidence of union between the host bone and implant. Radiographic union was observed in seven out of eight host bone-implant interfaces in the BM-MSC group after 20 weeks. Similar results were found in the other experimental groups (AT-MSC group, 6/8; UCB-MSC group, 7/8; and WJ-MSC group, 7/8). In contrast, union between the host bone and implant was seen at only one out of eight interfaces in the control group after 20 weeks. The times at which osseous union at the host bone-implant interfaces appeared were similar among the experimental groups (Table 1). The control group was excluded from calculating this time because radiographic union was observed at only one interface. The time of the one union observed in the control group was 16 weeks.

### Histological and histomorphometric analysis

In all experimental groups, substantial bone formation was observed throughout the bone defect (Fig. 7). Newly formed bone was primarily observed on the surface of intact β-TCP particles. In addition, cortical continuity was identified by the lack of a distinct boundary between host bone and newly formed bone in these experimental groups. Newly woven and lamellar bones in direct contact with the β-TCP particles and osteocytes embedded within the bone matrix were observed at higher magnification (×200). Hematopoiesis was also observed within the bone matrix. Overall, the histological findings were similar among the experimental groups. In contrast, the control group treated with β-TCP alone had minimal new bone formation throughout the implant, and continuity between native bone and the implant was absent.

The bone formation capacity was assessed in all groups by measuring areas of newly formed bone with histomorphometry. Percentages of NBA to TA were significantly higher for the experimental groups treated with the canine MSCs from various sources compared to the control group (Table 2, $p < 0.05$). However, the amounts of new bone formed were not significantly different among the experimental groups. The RTA to TA percentages for all groups were not significantly different.

**Table 2.** Histomorphometric analysis of new bone formation and residual β-TCP in the implanted areas

| Group | NBA/TA (%) | RTA/TA (%) |
|---|---|---|
| Control | 22.20 ± 1.74 | 38.62 ± 3.10 |
| AT-MSC | 33.90 ± 4.31* | 33.11 ± 1.77 |
| BM-MSC | 33.56 ± 8.09* | 31.11 ± 12.60 |
| UCB-MSC | 42.79 ± 8.00* | 32.46 ± 11.33 |
| WJ-MSC | 39.58 ± 8.10* | 30.42 ± 7.86 |

Data are presented as the mean ± SD. *Significantly different compared to the control ($p < 0.05$). NBA: newly formed bone area, RTA: residual β-TCP area, TA: total implanted area.

## Discussion

For the therapeutic use of MSC-based bone tissue engineering, it is essential to identify suitable conditions to promote osteogenesis. In the present study, we focused on MSCs from different sources to establish suitable conditions for bone repair. A few reports have recently compared the osteogenic abilities of MSCs derived from different tissues [11,19]. However, these studies evaluated osteogenesis only by performing *in vitro* assays or *in vivo* ectopic implantation. *In vitro* osteogenesis or *in vivo* ectopic bone formation may not represent the actual osteogenic potential of MSCs transplanted into a bone defect. Therefore, the current study used not only an *in vitro* assay but also *in vivo* orthotopic implantation to investigate bone formation by various types of MSCs.

Our *in vitro* osteogenic study showed that AT-MSCs and UCB-MSCs had a greater osteogenic potential than BM-MSCs and WJ-MSCs although subcultures of all types of MSCs formed sufficient bone matrix under osteogenic differentiation conditions. However, all MSCs induced substantial *in vivo* bone formation and significant differences in the levels of bone formation promoted by the various MSCs were not observed. These findings indicate the osteogenic potential observed *in vitro* and *in vivo* can be slightly different for each type of MSCs. This hypothesis is supported by previous reports demonstrating that findings from an *in vitro* osteogenic differentiation

assay correlate poorly with the results of an *in vivo* osteogenic differentiation assay [5,11]. These reports also suggested that confirming osteogenic potential using an *in vivo* rather than an *in vitro* system is more appropriate to ascertain bone regeneration abilities.

Differences of osteogenic potential as measured by the *in vitro* and *in vivo* experiments can be potentially explained by several factors. First, vascularization may have contributed to homeostasis of the microenvironment that promoted MSC survival and bone formation. Some reports proposed that the initial presence of MSCs stimulates bone formation by inducing vascularization [1,7,21]. MSCs are generally known to secrete substantial quantities of VEGF that plays a central role in the angiogenic response. Our present study measured VEGF production *in vitro* to determine the ability of each MSC type to promote neovascularization. BM-MSCs secreted significantly greater quantities of VEGF compared to other MSCs while AT-MSCs produced the lowest amount of VEGF. In contrast, bone matrix deposits formed by AT-MSCs under osteogenic conditions were larger than those of other MSCs, and BM-MSCs had a weaker osteogenic differentiation capability compared to AT-MSCs and UCB-MSCs. However, new bone was formed in a similar manner by all types of MSCs in the *in vivo* osteogenic assay. Based on these results, we can speculate that *in vivo* bone formation may be affected by the ability of MSCs to facilitate neovascularization. Indeed, hematopoietic tissues were observed more frequently within the bone matrix in histological sections from all experimental groups compared to the control group.

MSCs may also affect bone formation by releasing factors that stimulated the induction and migration of cells in the surrounding bone [7,26]. In reality, all bone healing process cannot be directly influenced by osteogenic differentiation of the transplanted cells. According to a previous report that investigated a transplantation model of live bone grafts from Rosa26A mice [36], only 70% of the induced osteogenesis on the graft depended on the expansion and differentiation of the donor progenitor cells. Furthermore, a previous study from our laboratory revealed that significant levels of cytokines released by canine UCB-MSCs 1 day after implantation can enhance bone regeneration [7].

Finally, interactions between MSCs and extracellular microenvironments may influence the fate of the cells. Local tissue microenvironments can affect stem cell attachment and migration, presentation of chemical and physical cues, and the binding of soluble factors [17,34]. These three different possibilities may have caused all types of MSCs to have similar levels of osteogenic potential *in vivo* and different degrees of osteogenic potential *in vitro*.

In the present study, allogenic MSCs were used to regenerate bone in long-bone defects with critical sizes. This may raise the issue of a possible adverse reaction or eventual rejection of the allogenic MSCs. However, previous studies have indicated that MSCs may be immune-privileged cells [2,4]. A previous *in vivo* orthotopic investigation demonstrated that allogenic MSCs do not provoke adverse immune responses, and are present in newly forming bone tissues when implanted into critical-sized bone defects in dogs without the use of immunosuppressive therapies [2]. In the present study, we showed that allogenic MSCs could enhance bone regeneration in critical-sized canine segmental defects without immunosuppressive therapies. The amounts of bone formed throughout the implants loaded with allogenic MSCs were significantly greater than those formed with cell-free implants. Thus, our study demonstrated the potential clinical application of allogenic MSCs for bone repair procedures.

BM-MSCs have been mainly used with biomaterials as a cell source for bone engineering. However, BM harvesting is a laborious and traumatic procedure, and the number and differentiation potential of the MSCs decrease with increasing age of the MSC donor [23]. Therefore, interest in the possibility of obtaining MSCs from other tissue sources has increased. In our study, AT, UCB, and WJ were used to obtain MSCs, and we measured the osteogenic potential of these cells to determine if they can be used as alternatives for BM-MSCs. The main advantages of AT-MSCs are that these cells are easy to obtain, are available in substantial quantities, and can be harvested with no risk of donor site morbidity. In addition, AT-MSCs grow stably *in vitro* and have a high expansion rate [32]. AT-MSCs were also shown in the present study to have a higher proliferation potential than the other types of MSCs. UCB-MSCs and WJ-MSCs can also be harvested painlessly without the risk of patient morbidity, maintain stemness *in vitro*, and are immune-privileged cells with surface characteristics capable of overcoming rejection [15,27]. In addition, UCB-MSCs have a significantly greater osteogenic potential *in vitro* compared to BM-MSCs according to a previous report [10]. Similarly, results of the *in vitro* assays performed in the present study indicated that UCB-MSCs possessed a greater osteogenic potential than BM-MSCs.

In conclusion, we demonstrated that AT-MSCs, UCB-MSCs, and WJ-MSCs have many advantages that make these cells ideal for bone repair procedures. These cells also possess a degree of osteogenic potential similar to that of BM-MSCs. Our findings suggest that AT-MSCs, UCB-MSCs, and WJ-MSCs are promising types of stem cells for bone regeneration techniques and can be used in place of BM-MSCs.

## Acknowledgments

This work was supported by the National Research Foundation of Korea (NRF) grant funded by the Korean government (MEST) (2009-0077045) and the Next-Generation BioGreen 21 program (Nos. P J008030 and J008032), Rural Development Administration, Korea.

## References

1. **Al-Khaldi A, Eliopoulos N, Martineau D, Lejeune L, Lachapelle K, Galipeau J.** Postnatal bone marrow stromal cells elicit a potent VEGF-dependent neoangiogenic response *in vivo*. Gene Ther 2003, **10**, 621-629.
2. **Arinzeh TL, Peter SJ, Archambault MP, van den Bos C, Gordon S, Kraus K, Smith A, Kadiyala S.** Allogeneic mesenchymal stem cells regenerate bone in a critical-sized canine segmental defect. J Bone Joint Surg Am 2003, **85**, 1927-1935.
3. **Arthur A, Zannettino A, Gronthos S.** The therapeutic applications of multipotential mesenchymal/stromal stem cells in skeletal tissue repair. J Cell Physiol 2009, **218**, 237-245.
4. **Bartholomew A, Sturgeon C, Siatskas M, Ferrer K, McIntosh K, Patil S, Hardy W, Devine S, Ucker D, Deans R, Moseley A, Hoffman R.** Mesenchymal stem cells suppress lymphocyte proliferation in vitro and prolong skin graft survival in vivo. Exp Hematol 2002, **30**, 42-48.
5. **Bianco P, Kuznetsov SA, Riminucci M, Robey PG.** Postnatal skeletal stem cells. Methods Enzymol 2006, **419**, 117-148.
6. **Bruder SP, Kraus KH, Goldberg VM, Kadiyala S.** The effect of implants loaded with autologous mesenchymal stem cells on the healing of canine segmental bone defects. J Bone Joint Surg Am 1998, **80**, 985-996.
7. **Byeon YE, Ryu HH, Park SS, Koyama Y, Kikuchi M, Kim WH, Kang KS, Kweon OK.** Paracrine effect of canine allogenic umbilical cord blood-derived mesenchymal stromal cells mixed with beta-tricalcium phosphate on bone regeneration in ectopic implantations. Cytotherapy 2010, **12**, 626-636.
8. **Cancedda R, Giannoni P, Mastrogiacomo M.** A tissue engineering approach to bone repair in large animal models and in clinical practice. Biomaterials 2007, **28**, 4240-4250.
9. **Caplan AI, Bruder SP.** Mesenchymal stem cells: building blocks for molecular medicine in the 21st century. Trends Mol Med 2001, **7**, 259-264.
10. **Chang YJ, Shih DT, Tseng CP, Hsieh TB, Lee DC, Hwang SM.** Disparate mesenchyme-lineage tendencies in mesenchymal stem cells from human bone marrow and umbilical cord blood. Stem Cells 2006, **24**, 679-685.
11. **Cho W, Nam S, Jang J, Lee E, Lee E, Son Y.** Comparative evaluation of differentiation potentials of various stem cells from mesenchymal tissue origin. Tissue Eng Regen Med 2010, **7**, 355-361.
12. **Ciapetti G, Ambrosio L, Marletta G, Baldini N, Giunti A.** Human bone marrow stromal cells: in vitro expansion and differentiation for bone engineering. Biomaterials 2006, **27**, 6150-6160.
13. **Dragoo JL, Samimi B, Zhu M, Hame SL, Thomas BJ, Lieberman JR, Hedrick MH, Benhaim P.** Tissue-engineered cartilage and bone using stem cells from human infrapatellar fat pads. J Bone Joint Surg Br 2003, **85**, 740-747.
14. **Drosse I, Volkmer E, Capanna R, De Biase P, Mutschler W, Schieker M.** Tissue engineering for bone defect healing: an update on a multi-component approach. Injury 2008, **39** (Suppl 2), S9-S20.
15. **Gauthaman K, Venugopal JR, Yee FC, Biswas A, Ramakrishna S, Bongso A.** Osteogenic differentiation of human Wharton's jelly stem cells on nanofibrous substrates *in vitro*. Tissue Eng Part A 2011, **17**, 71-81.
16. **Gregory CA, Gunn WG, Peister A, Prockop DJ.** An Alizarin red-based assay of mineralization by adherent cells in culture: comparison with cetylpyridinium chloride extraction. Anal Biochem 2004, **329**, 77-84.
17. **Haque MA, Nagaoka M, Hexig B, Akaike T.** Artificial extracellular matrix for embryonic stem cell cultures: a new frontier of nanobiomaterials. Sci Technol Adv Mat 2010, **11**, 014106.
18. **Hattori H, Masuoka K, Sato M, Ishihara M, Asazuma T, Takase B, Kikuchi M, Nemoto K, Ishihara M.** Bone formation using human adipose tissue-derived stromal cells and a biodegradable scaffold. J Biomed Mater Res B Appl Biomater 2006, **76**, 230-239.
19. **Hayashi O, Katsube Y, Hirose M, Ohgushi H, Ito H.** Comparison of osteogenic ability of rat mesenchymal stem cells from bone marrow, periosteum, and adipose tissue. Calcif Tissue Int 2008, **82**, 238-247.
20. **Janicki P, Kasten P, Kleinschmidt K, Luginbuehl R, Richter W.** Chondrogenic pre-induction of human mesenchymal stem cells on beta-TCP: enhanced bone quality by endochondral heterotopic bone formation. Acta Biomater 2010, **6**, 3292-3301.
21. **Kaigler D, Krebsbach PH, Polverini PJ, Mooney DJ.** Role of vascular endothelial growth factor in bone marrow stromal cell modulation of endothelial cells. Tissue Eng 2003, **9**, 95-103.
22. **Kasten P, Vogel J, Luginbühl R, Niemeyer P, Tonak M, Lorenz H, Helbig L, Weiss S, Fellenberg J, Leo A, Simank HG, Richter W.** Ectopic bone formation associated with mesenchymal stem cells in a resorbable calcium deficient hydroxyapatite carrier. Biomaterials 2005, **26**, 5879-5889.
23. **Kern S, Eichler H, Stoeve J, Klüter H, Bieback K.** Comparative analysis of mesenchymal stem cells from bone marrow, umbilical cord blood, or adipose tissue. Stem Cells 2006, **24**, 1294-1301.
24. **Kikuchi M, Koyama Y, Yamada T, Imamura Y, Okada T, Shirahama N, Akita K, Takakuda K, Tanaka J.** Development of guided bone regeneration membrane composed of $\beta$-tricalcium phosphate and poly (L-lactide-*co*-glycolide-*co*-ε-caprolactone) composites. Biomaterials 2004, **25**, 5979-5986.
25. **Kon E, Muraglia A, Corsi A, Bianco P, Marcacci M, Martin I, Boyde A, Ruspantini I, Chistolini P, Rocca M, Giardino R, Cancedda R, Quarto R.** Autologous bone

marrow stromal cells loaded onto porous hydroxyapatite ceramic accelerate bone repair in critical-size defects of sheep long bones. J Biomed Mater Res 2000, **49**, 328-337.

26. **Kruyt MC, Dhert WJA, Oner FC, van Blitterswijk CA, Verbout AJ, de Bruijn JD.** Analysis of ectopic and orthotopic bone formation in cell-based tissue-engineered constructs in goats. Biomaterials 2007, **28**, 1798-1805.
27. **Lee OK, Kuo TK, Chen WM, Lee KD, Hsieh SL, Chen TH.** Isolation of multipotent mesenchymal stem cells from umbilical cord blood. Blood 2004, **103**, 1669-1675.
28. **Mastrogiacomo M, Corsi A, Francioso E, Di Comite M, Monetti F, Scaglione S, Favia A, Crovace A, Bianco P, Cancedda R.** Reconstruction of extensive long bone defects in sheep using resorbable bioceramics based on silicon stabilized tricalcium phosphate. Tissue Eng 2006, **12**, 1261-1273.
29. **Petite H, Viateau V, Bensaïd W, Meunier A, de Pollak C, Bourguignon M, Oudina K, Sedel L, Guillemin G.** Tissue-engineered bone regeneration. Nat Biotechnol 2000, **18**, 959-963.
30. **Pittenger MF, Mackay AM, Beck SC, Jaiswal RK, Douglas R, Mosca JD, Moorman MA, Simonetti DW, Craig S, Marshak DR.** Multilineage potential of adult human mesenchymal stem cells. Science 1999, **284**, 143-147.
31. **Rauch C, Brunet AC, Deleule J, Farge E.** $C_2C_{12}$ myoblast/osteoblast transdifferentiation steps enhanced by epigenetic inhibition of BMP2 endocytosis. Am J Physiol Cell Physiol 2002, **283**, C235-C243.
32. **Schäffler A, Büchler C.** Concise review: adipose tissue-derived stromal cells--basic and clinical implications for novel cell-based therapies. Stem Cells 2007, **25**, 818-827.
33. **Woodbury D, Reynolds K, Black IB.** Adult bone marrow stromal stem cells express germline, ectodermal, endodermal, and mesodermal genes prior to neurogenesis. J Neurosci Res 2002, **69**, 908-917.
34. **Yang F, Cho SW, Son SM, Hudson SP, Bogatyrev S, Keung L, Kohane DS, Langer R, Anderson DG.** Combinatorial extracellular matrices for human embryonic stem cell differentiation in 3D. Biomacromolecules 2010, **11**, 1909-1914.
35. **Yuan J, Cui L, Zhang WJ, Liu W, Cao Y.** Repair of canine mandibular bone defects with bone marrow stromal cells and porous $\beta$-tricalcium phosphate. Biomaterials 2007, **28**, 1005-1013.
36. **Zhang X, Xie C, Lin ASP, Ito H, Awad H, Lieberman JR, Rubery PT, Schwarz EM, O'Keefe RJ, Guldberg RE.** Periosteal progenitor cell fate in segmental cortical bone graft transplantations: implications for functional tissue engineering. J Bone Miner Res 2005, **20**, 2124-2137.